

External Grant Award Number: 08HQGR0137 and 08HQGR0136

Submitted: June 2010

Title: Collaborative Research with California State Polytechnic University, Pomona, and URS Corporation: Near Real-Time Determination of Focal Mechanisms and Depths of Large Worldwide Earthquakes

Time covered by the Award: 09/01/2008 through 03/31/2010

Authors:

Jascha Polet
Department of Geological Sciences
California State Polytechnic University
Pomona, CA 91768
Tel.: (909) 869-3459
E-mail: jpolet@csupomona.edu

Hong Kie Thio
URS Group Inc.
566 El Dorado Street, 2nd floor
Pasadena, CA 91101
Tel.: (626) 449-7650
E-mail: hong_kie_thio@urscorp.com

Abstract

Modern day broadband seismic instrumentation and real-time data availability allow us to monitor the Earth in greater detail and over a much wider bandwidth than traditionally possible. The near real-time analysis of the source characteristics of earthquakes is crucial for seismic hazard mitigation and efficient emergency response. We have developed an algorithm for the continuous determination of locations and magnitudes for global earthquakes down to magnitude 5.5 using long period surface wave data from global seismic arrays and have recently extended its functionality by developing an additional module that determines moment tensor solutions.

The original algorithm uses a Rayleigh wave back-projection approach and consists of a continuous progressive conversion of time series into spectrograms and the mapping of those spectrograms onto a grid of locations and origin times. It distinguishes itself by its straightforward adaptation into a routine monitoring system and its constant load approach, thus avoiding potential problems with intense earthquake sequences. This method can provide a reliable estimate of the moment of global earthquakes without saturating and thus is particularly useful for large earthquakes, which have proven to be difficult to analyze in near real-time using traditional body wave techniques. It can also act as a backup to the current NEIC monitoring software and detect events that are missed, or underestimated, by the current system. Particularly important in this regard are the so-called “tsunami” earthquakes, long period earthquakes that excite anomalously large tsunami and are underestimated by the standard body wave based techniques, but are correctly identified as potentially hazardous events by our analysis system. Other events that are frequently underestimated as a result of body wave analysis, but correctly assessed using our surface wave back-projection technique, are slow oceanic transform earthquakes. Our newly added calculation of moment tensors and earthquake depths employs the same spectral parameters already calculated for the determination of earthquake magnitudes and locations.

We have implemented a pilot system that calculates the location and magnitude of global earthquakes in a fully automatic manner, without the need for a human operator to select or process data, at the National Earthquake Information Center (NEIC) of the United States Geological Survey (USGS). This system currently runs every 24 hours and produces a movie of its results that is made available for viewing on a (at the moment not publically accessible) web site. We have analyzed the results of this prototype system for the time period of March 2009 to April 2010, to assess its performance and calibrate the produced magnitudes with those in the final NEIC earthquake catalog. Our analysis shows that the system performs well for events greater than magnitude 5.5 and determines reliable magnitudes and locations for global events shallower than 150 km in depth. We have also tested a new extension to this system to determine earthquake moment tensors and depths, and have found that it performs well for very large events, but will require changes to the current system to be functional for smaller events. The phase errors that are introduced due to the currently implemented relatively coarse grid and time spacing negatively impact the inversion of moment tensors from azimuthal phase and amplitude variations. However, this problem may be addressed by locally re-sampling the grid to smaller size and using smaller time steps for the space and time period around detected events.

Introduction

The deployment of digital broadband seismographs around the world, and the introduction of near real-time data collection have revolutionized seismology and opened up new ways of monitoring seismic activity throughout the world. These developments have allowed us

to rethink the way we view seismic events, and how we study them. We have developed an alternative method of monitoring seismic activity at long periods, which complements existing earthquake location and analysis techniques used at the USGS NEIC.

Limitation of traditional monitoring techniques

Most current monitoring schemes rely heavily on time-tested routines that are based on short-period signals, i.e. P and S wave arrivals, and are triggered by relatively high amplitude arrivals at one or more stations. Typically, these methods yield a location for the hypocenter and the origin time. More detailed analysis is then usually performed using waveform inversions that determine the seismic moment, moment tensor, and, in some cases, the centroid location. These short period methods generally produce accurate and reliable results, but they have also been known to fail for a variety of reasons, most significantly due to the long period character of earthquakes of large size, but also because of the anomalously “slow” nature of certain earthquakes. For instance, in the case of the destructive 2004 Sumatra earthquake, initial magnitude estimates yielded magnitudes (8.5) that significantly underestimated the true size of the event and only after several hours was a more accurate magnitude (9.0) obtained. Such a delay may have severe consequences for hazard mitigation such as tsunami early warning systems. Another problem with the use of short period seismic analysis methods is the occurrence of slow earthquakes, which may occur on oceanic transform faults (Ihmlé and Jordan, 1994; McGuire et al., 1996) and in a shallow subduction zone setting (Polet and Kanamori, 2000), with the latter type of event often particularly tsunamigenic. Due to their anomalously low corner frequency, these earthquakes tend to saturate the different magnitude scales at a lower level than regular earthquakes. For instance, for the 1994 Java earthquake the body wave magnitude (m_b) and surface wave magnitude (M_s) reported in the monthly NEIC bulletin are 5.7 and 7.1 respectively, whereas the moment magnitude (M_w) is 7.9 (Polet and Thio, 2003). A similar discrepancy exists for the more recent 2006 Java tsunami earthquake, about 600 km in distance from the 1994 event. The body wave magnitude of these earthquakes would not set off any alarm or require special attention from monitoring personnel. However, both events caused destructive tsunamis in Java with run-ups as high as 10 m. Similarly anomalously slow earthquakes have been observed in other subduction zones (Polet and Kanamori, 2000). Since our proposed methodology both extends traditional methods, and also overlaps with them, it can serve both as an analysis tool for great and anomalous earthquakes, detect small earthquakes based on surface wave data and act as a backup for “regular” events, also detectable using body waves.

Moreover, to obtain a rapid and accurate assessment of the hazard posed by an earthquake, knowing its magnitude alone is not sufficient. The depth and mechanism of an earthquake play an important part in determining its potential for causing damage and casualties. For example, the $M_w=6.3$ Java earthquake of May 26, 2006, was a shallow strike-slip event that killed at least 5,749 people, injured 38,568 and left as many as 600,000 people displaced in the Bantul-Yogyakarta area (<http://earthquake.usgs.gov/eqcenter/recenteqsww/Quakes/usneb6.php>). This event occurred in a region that also experiences subduction zone earthquakes at greater depths (70 km or deeper). Clearly, a subduction zone earthquake of the same magnitude at these depths would not have caused as much destruction. Even with a poorly resolved depth, knowledge of the strike-slip mechanism of this event would have helped in the identification of its tectonic environment, as it does not reflect slip on the interface between subducting and overriding plates. Similarly, the depth and mechanism of an earthquake are important factors in its tsunamigenesis. Shallow events with mechanisms indicating great vertical uplift of the ocean floor are more efficient at exciting tsunami waves than deeper or strike-slip earthquakes. Therefore, to develop a full picture of the hazard posed by an earthquake, due to either seismic shaking or a possible tsunami following the event, we also need to know its mechanism and depth, in addition to its location, origin time and moment magnitude.

Alternative methods of seismic monitoring

In recent years, the use of long period waves has proven to be quite effective in detecting and locating earthquakes. Beroza and Jordan (1990) used normal modes to search for slow and silent earthquakes, and detected several such events, even with the limited station distribution available to them at that time. Shearer (1994) developed a method using very long-period surface waves to detect and locate earthquakes on a global scale and applied it successfully to 11 years worth of IDA data, thereby detecting events ($M_w > 5.5$) that were not included in any of the earthquake catalogs because of their slow nature. Ekström and Nettles (2002) developed a surface wave detector/locator system with which they detected, among others, glacial earthquakes that are depleted in high frequency signals. Others have also found signals related to slow glacial earthquakes, glacier movements and landslides using similar methods (Ekström et al., 2003; Chen et al., 2008) and very-low-frequency (~ 20 sec) earthquakes with $M_w=3.1-3.5$ have been detected in the transition zone of the subducting plate interface in the Nankai subduction zone (Ito et al., 2007). Kawakatsu (1998, 2002) developed a more comprehensive method solving not only for location and time, but also for mechanism. A similar method was implemented for earthquakes in California by Tajima et al. (2002).

In the last few years, significant advances have been made in the modeling of earthquake rupture processes by using back-projection methods (Ishii et al., 2005; Walker et al., 2005) of body waves from stations from either regional or worldwide networks. These new technologies possibly represent a significant step forward in the analysis of seismic source processes, however, at this point in time their application is fairly sophisticated and involves the use of significant a-priori knowledge about the fault geometry.

The aforementioned methods have all been successful in detecting and analyzing seismic activity. However, most do not lend themselves easily to implementation on a routine basis in near real-time. What sets our method apart is its simplicity both in terms of algorithm and near real-time operation.

Basic methodology

Continuous systems have several advantages over more traditional triggered methodologies. One advantage of using a continuous method is that it does not rely on having a hypocentral location provided to it before it can work. Although the short period systems that are used to determine these hypocentral parameters generally perform very well, over the last few years it has become obvious that their use may be limited in the case of truly extraordinary events, like the 2004 Sumatra-Andaman Islands earthquake, or other unusual events like slow tsunami earthquakes. More in general, a real-time system that consists of as few modules as possible is good design practice, since it limits the number of possible points of failure.

The original locator system implements a method similar to measuring arrival times of seismic phases and mapping them back to a location and origin time. An analogy with body wave methods is that we measure the arrival times of surface waves at different periods that propagate at different speeds, which is the equivalent of using multiple body wave phases (direct P and S) to constrain the distance from the source to the station and the origin time. An important distinction is that with high frequency methods the arrival of the first break is measured, corresponding to the onset of an earthquake rupture. With our proposed method, we measure the main arrival of energy in a particular frequency band. The resultant location is therefore more indicative of the centroid of an earthquake.

The more recently developed module that determines the depth and mechanism (moment tensor) of the earthquake consists of an examination of the global stacked amplitude grid as a function of time, and retrieval of the original complex spectral measurements that these amplitudes are based on, for the grid points that correspond to the maximum in stacked amplitude on the globe. These measurements are then used in an inversion for a moment tensor (MT) and

depth for those grid points. The depth is determined by comparing the variance reduction we obtain for the fit of the measured spectra to the predicted radiation pattern and finding the depth at which a maximum is achieved. The MT module can also feed back information into the locator, in that a high variance reduction of the inversion signifies a ‘real’ earthquake has occurred and can therefore be used as an additional trigger for event declaration.

In the next sections of this report, we will first describe the underlying methodology of the locator system that we have developed and installed at the NEIC and show examples of its performance. Subsequently we will describe our results of the performance analysis of our system and our progress on implementing the extension to this system to compute depths and moment tensors.

Indirect mapping

Our solution to detecting events using waveforms from an array consists of a simple continuous mapping of the surface wave arrivals from different stations and different periods onto a (global) grid, using group velocity based travel time corrections. The method is very straightforward, and consists of three steps. The first is akin to the traditional method of measuring dispersion using a sliding window, which results in a spectrogram (Figure 1) with amplitude as a function of period and arrival time $F(\tau, T)$. These spectrograms can then be mapped into origin time (τ_0) and distance (R_0) for every individual station:

$$(1) \quad G_j(\tau_0, R_0) = \sum_{i=1}^{nT} F_j\left(\tau + \frac{R_0}{u(T_i)}, T_i\right)$$

where R_0 is the target distance, $u(T_i)$ the group velocity, F_j the spectrogram for station j and G_j the time-distance function. Function G will then show localized maxima for every time-distance pair corresponding to a seismic event. There is an equivalent in the high-frequency seismology, where, if the P and S arrival time are measured at a station, we would have a rough estimate of the origin time and the distance from the station to the event, since the separation between direct P and direct S is unique for every distance, if we neglect the depth of the event. In our current algorithm, the localized maxima in G are not used to identify events explicitly. Instead we continue with a final mapping of G into a three-dimensional space spanned by the geographic coordinates and origin time:

$$(2) \quad H(x, y, \tau_0) = \sum_{j=1}^{nStations} G_j(\tau_0, R_0(x, y))$$

where $R_0(x, y)$ is the distance from point (x, y) , the target location, to the station. Seismic events are then identified as local maxima of function H both in space as well as time.

Grid and data

In order to facilitate the analysis, it is advantageous to use a gridding scheme with cells of equal size. On a sphere, this is difficult to achieve, but a good approximation is to use the cubed-sphere transformation (Ronchi et al., 1996). In this transformation, the entire globe is divided into six equal sectors, which are then projected on square flat surfaces. These surfaces form the sides of a cube, hence the name. The main attraction for this transformation is the fact that it provides a convenient framework for solving differential equations on a sphere, but we use it solely for the ease of achieving near-uniform grid coverage.

Depending on the period range of interest, most of the broadband data that is commonly gathered today is suitable to be included in this method. When analyzing very long periods (300

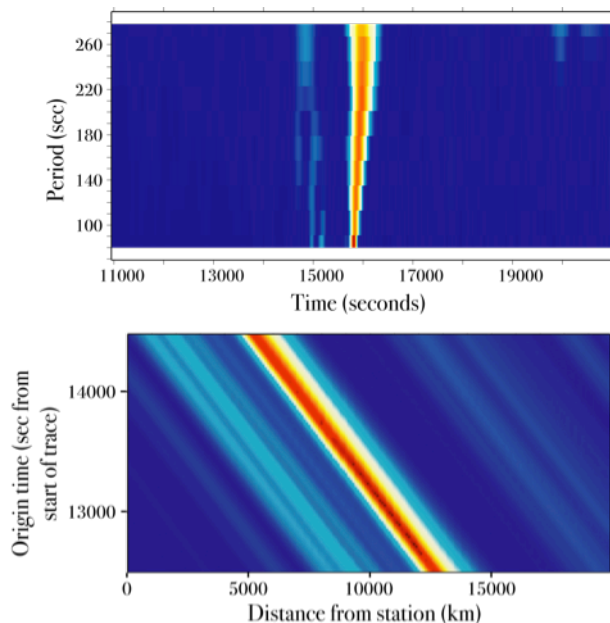


Figure 1: Top panel shows spectrogram with surface wave arrivals and dispersion clearly visible. Transformation to distance and origin time is shown in bottom panel.

sec), we use data from STS-1 or equivalent instruments, since their response is flat (in velocity) for the entire spectrum of interest. In fact, higher sampling rates would only needlessly slow down the procedure without adding any more information. The demands on data throughput with this system are therefore minimal, compared to traditional methods, which use data at a rate of 80 Hz.

Real-time operation

The algorithm can easily be adapted for a continuous near real-time environment. The basic premise is that a time lag is built into the locator, so that we allow surface waves to be included that have traveled the distance equivalent to the time lag, or less. For instance, if we want all global stations to be included for any possible event, the time lag should be set so that the waves arriving from the antipode are included. For a long period surface wave this would amount to over 1.5 hours. Given a dense enough coverage, this is not necessary, and even with the limited number of stations used in some of our examples we never used a lag time of more than an hour. The version of the system that is currently operational at the NEIC uses a lag time of 30 minutes. Therefore, this implemented proto-type produces results that are the equivalent to those of a near real-time operational system, even if it currently only runs in batch mode, every 24 hours.

Since the spectrogram can be continuously updated, the sliding window analysis would not need any modifications for true near real-time use, and it would even be possible to replace the Fourier Transform with recursive filter and envelope functions. For the mappings of equation 2 we would choose the target time τ_0 to be the current time minus the lag time.

Evaluation of system performance

We initially tested the performance of the algorithm on several specific events and days of data. Two of these tests were carried out for the 2004 great Sumatra earthquake and the 1994 Java tsunami earthquake. When we found that the system performed well, we proceeded to install the surface wave locator algorithm as described earlier on computers at the NEIC in Golden, where it is currently operated in batch-mode for testing and development purposes in cooperation with USGS staff. This proto-type system can be run at any point in time for a specified time

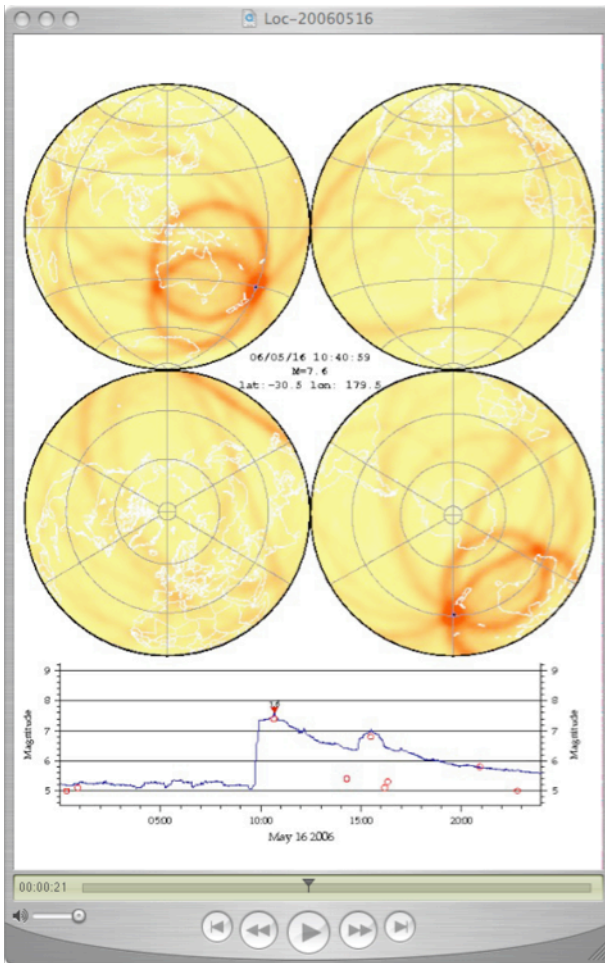


Figure 2: Screen shot of the proto-type tool for use of locator by analysts. The software can be run at any point in time and will analyze a requested time period of data. The system produces a set of images that are subsequently used to generate a movie of the stacked amplitude across the globe for the specified time period (top panels). The movie will enable the analyst to quickly identify false “events” that are due to instrumental noise, since these generate very characteristic patterns. The numbers in the center of the four panels show the magnitude and location of the maximum of the stacked amplitude, a time trace of which is shown in the bottom panel, together with the catalog predictions.

period and incorporates the current NEIC catalog of events in its display to enable the comparison of the locator results with the results from the short-period real-time system (see Figure 2 for a screenshot of this proto-type).

We will first describe the results of our initial tests, will then proceed to discuss the performance of the NEIC prototype system and will finally show preliminary moment tensor inversion results.

Anomalous events: 1994 Java earthquake

Even with a lag-time of only 900 seconds (15 minutes) the surface wave back-projection algorithm is able to obtain an accurate location and moment for the 1994 Java earthquake (Figure 3 and Table 1). For this event the body wave magnitude (m_b) and surface wave magnitude (M_s) reported in the monthly NEIC bulletin are 5.7 and 7.1 respectively, whereas the moment magnitude (M_w) is 7.9. This event excited unusually large local tsunami, possibly due to an uncommonly shallow rupture, which may also be the cause of its slow character due to the low rupture velocity through the shallow sediments. Similar slow tsunami earthquakes have occurred in other shallow subduction zones (Polet and Kanamori, 2000), such as the 1992 Nicaragua earthquake. More recently, in 2006, another slow event occurred in the Java subduction zone; again its magnitude was underestimated using conventional body and surface wave techniques.

The 2004 Sumatra-Andaman earthquake

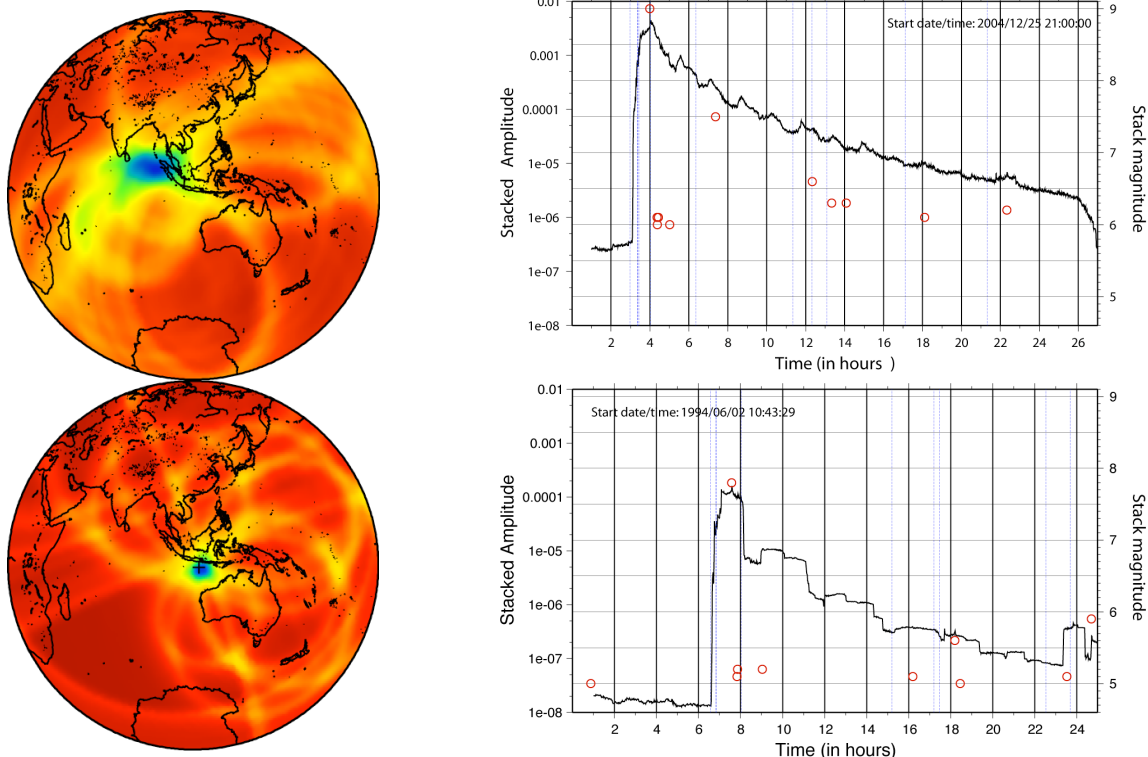


Figure 3. Locator results for the 2004 Sumatra-Andaman earthquake (top panels) and the 1994 slow Java earthquake (bottom panels). We used a time lag of only 900 sec for the Java earthquake. The resulting location for the Java event is very close to the Global CMT centroid solution, as is the magnitude of 7.9. Thus, within 15 minutes, an accurate location and moment are available, based on data from only 8 stations, none within 10° of the source. For the Sumatra earthquake, we used only 7 stations and a lag-time of 1800 seconds to determine a magnitude of 8.9.

The results for the 2004 Sumatra-Andaman event are also satisfactory (Figure 3 and Table 1), although in this case we used a lag-time of 1800 seconds due to the larger distance to the available stations. This earthquake is particularly difficult to analyze since the source time (600 seconds, Ammon et al., 2005) is actually longer than the longest period waves that we used. Nevertheless, we are able to obtain a location and moment that are consistent with the values that were obtained by more detailed analysis hours or days after the event. Our results for both the Java and Sumatra earthquake demonstrate the suitability of this method for the analysis of very large earthquakes or slow earthquakes. Preliminary results for the Aceh earthquake and the 2010 great Chilean earthquake (see movie at <http://neic.cr.usgs.gov/beta/slaqr/> usr:slaqr password:slaqr) also indicate that the locator may be able to map the propagation of a large rupture as a function of time.

Date	Time	Lat	Lon	M
1994/06/02	18:17:37	-10.4132	112.964	7.8
	18:18:50	-12.51	112.50	7.9
2004/12/26	00:58:53	3.295	95.982	9.0
	01:02:27	1.50	94.50	8.9

Table 1 Comparison of NEIC parameters and our results (bold italics) for the 1994 Java and 2004 Sumatra-Andaman events

Day-to-day operation

For our prototype system, we selected an initial list of 57 global stations on the basis of instrument quality and global coverage, with on average 45 traces used on any given time (due to data dropout and station availability issues). As a future improvement, we would like to create a dynamic station list, based on the daily long period station noise analysis parameters produced by Dr. McNamara from the NEIC, but this improvement has not been implemented yet in the prototype system. For a lag time of half an hour, every location on the globe will only be “in reach” of a limited number of stations, given the limited distance that the Rayleigh waves can propagate in that time period. Based on a maximum propagation distance of 5000 km, the station coverage “hit count” map shown in Figure 4 indicates that coverage of the globe is generally good, but as expected could be improved in the mid-Atlantic, southern Indian Ocean and Antarctica regions.

The prototype system can locate global events down to magnitude 5.5, or even lower, reliably and consistently. In Figure 5 we show, as an example, the results produced by the locator for a day with several large earthquakes in different locations across the globe. All four earthquakes were located within 300 km of the final NEIC catalog (with a coarse grid spacing of 1 degree), and the magnitudes were within 0.3 units of the final NEIC catalog magnitude. This particular example also shows a specific strength of the algorithm: the determination of a correct magnitude for slow oceanic transform earthquakes, in this case a magnitude 6.4 mid-Atlantic ridge event (C) that was initially determined to be a magnitude 5.2 by body wave techniques.

The prototype system has been operational at the NEIC since March 2009, running in batch mode every 24 hours with a lag time of half an hour. The results produced by this system are thus similar to those that would be produced if the system would be run in near real-time mode with the same lag time. Using the 13 months of results from this prototype system, we carried out a calibration of stacked amplitude as a function of final NEIC catalog moment magnitude. First we associated peaks in the stacked global amplitude with earthquakes in the

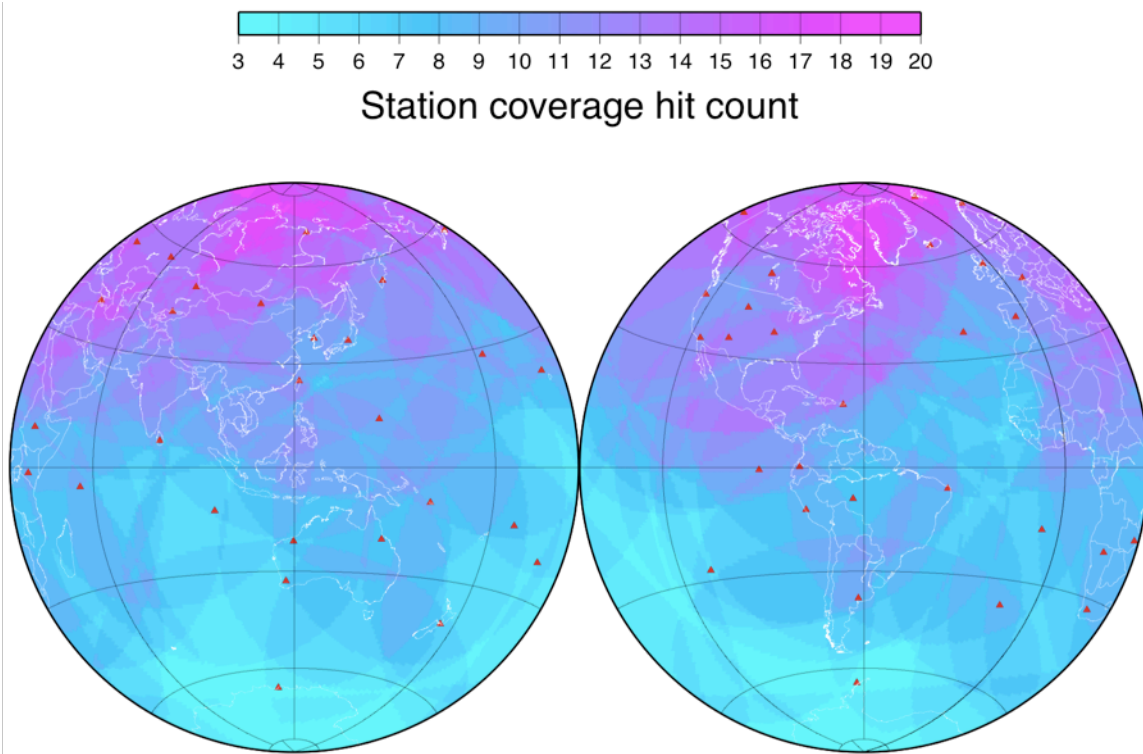


Figure 4: Station coverage of global earthquake grid, with stations shown as red triangles.

NEIC catalog, as obtained from the catalog search webpage at http://earthquake.usgs.gov/earthquakes/eqarchives/epic/epic_global.php. For the associated peaks, we created a database with the exact time of the peak (the time step of the analysis carried out by the prototype system is one minute), the location of the maximum stacked amplitude on

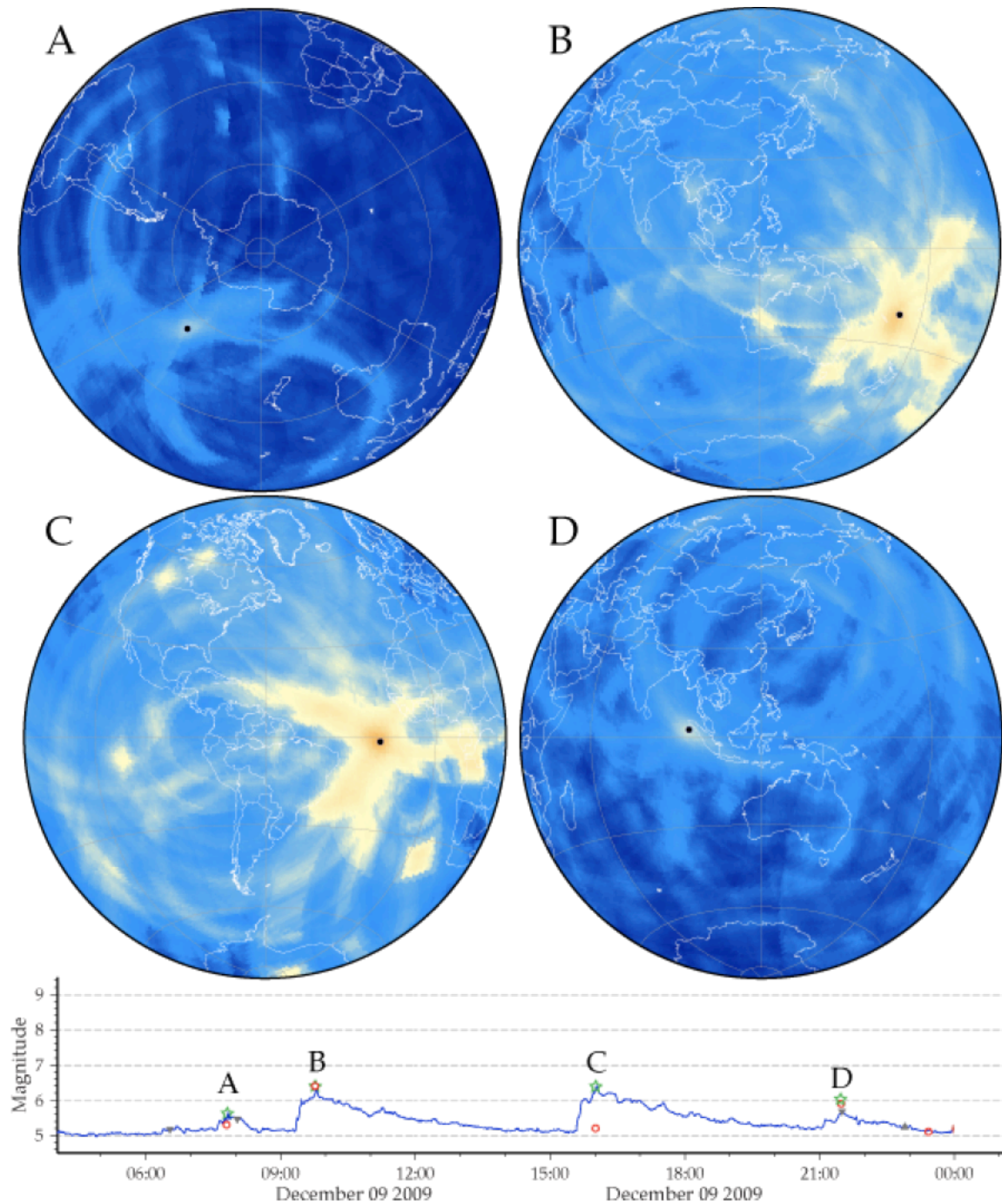


Figure 5: Example of locator results for a 20-hour period on December 9, 2009. Top panels shows stacked amplitudes on the global grid, with the black dot showing the location of the maximum amplitude for events A-D. Bottom graph shows the variation of the maximum of the stacked amplitude as a function of time, with the red circles showing the NEIC catalog magnitudes as available at the time the locator was run (8:00 UTC the next day) and the green stars the final NEIC magnitudes.

the globe (the grid spacing is approximately one degree) and the value of the maximum stacked amplitude. To only use suitable data in this calibration, we incorporate two different selection criteria. Based on a preliminary analysis of the data, we found that the magnitude of deep events was consistently underestimated. This is not surprising, given that the surface wave excitation of deep earthquakes is relatively low. Therefore, we only selected events from the final NEIC catalog that were shallower than 150 km for our calibration. Secondly, a disadvantage to using long period surface waves is the continued presence of high amplitude surface waves across the globe for a relatively long period of time after a large event has occurred. This effect appears as a “tail” to the peak in the maximum stacked amplitude trace, as can be seen in the bottom graph of Figure 5, for example. Due to this “tail” there is a period of time after a large event has occurred that any subsequent peaks due to smaller events will not be visible in the stacked amplitude. To determine the character of this drop-off in amplitude with time, we analyzed the temporal behavior for all events greater than 5.5 after normalizing the peak amplitude. The general shape of the drop-off agrees well across all magnitudes, although of course for smaller magnitude earthquakes the background “noise” level is reached much faster than for the larger events (see Figure 6). We performed a polynomial fit to the amplitude decay curve, shown in Figure 6, for events greater than 6.5, in order to be able to determine for each event in the final NEIC catalog whether it should be detectable above the noise level from earlier earthquakes. We then compared the peak amplitude determined by the system for each event to the amplitude predicted from earlier earthquakes and if the ratio between these two amplitudes was at least two (or no other earthquakes occurred in the 24 hours prior to the event), the event was classified as “detectable” and added to the calibration dataset. We will also be able to incorporate the results of this analysis in the system in the future to help assess the reliability of detected events based on previous seismicity, which should be particularly useful for aftershock sequences.

After removal of the deep earthquakes and “undetectable” events from the calibration dataset, we proceeded to perform a simple linear curve fit to the maximum stacked amplitude of the remaining events larger than magnitude 5.5. After one iteration, in which we removed outliers at more than 0.5 magnitude units from the curve fit, a calibration curve was determined (see Figure 7). The excellent fit of the data points to a straight line across the full magnitude range

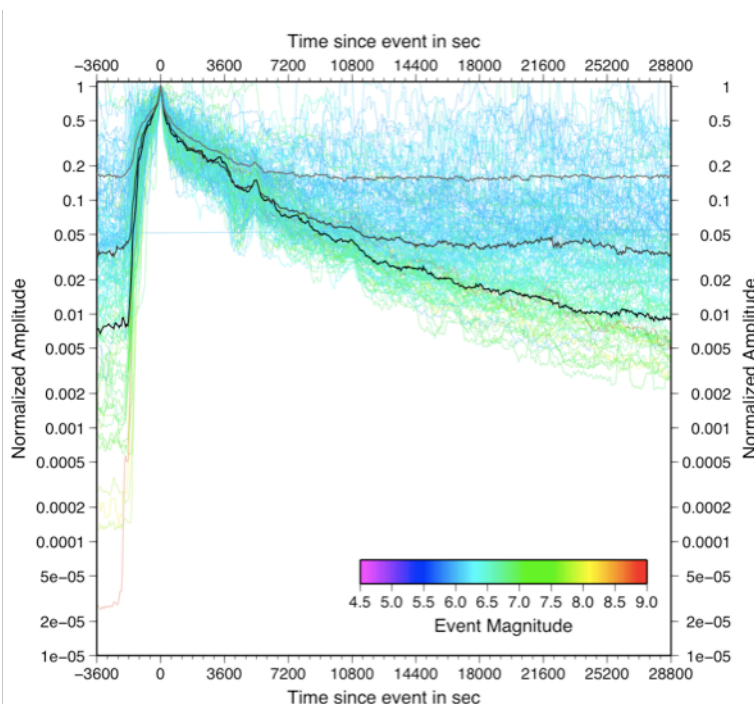


Figure 6: Amplitude decay in maximum stacked amplitude as a function of time since the occurrence of an earthquake. Three thick curves shown are medians for events with magnitude greater than 6.5 (bottom curve), greater than 6.0 (middle curve) and greater than 5.5 (top curve).

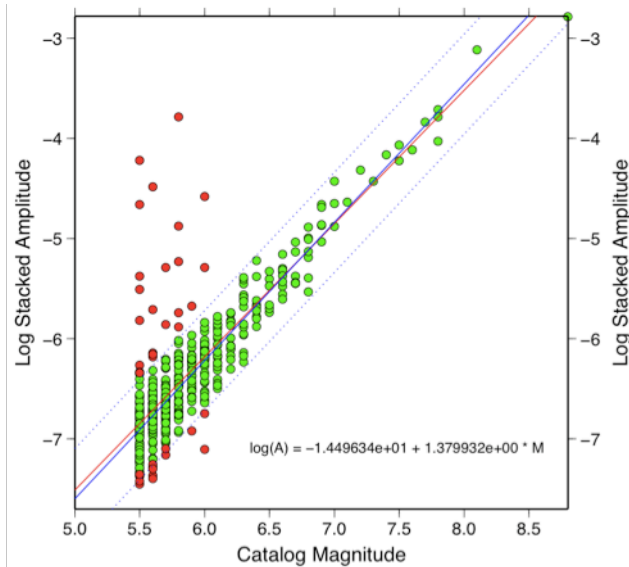


Figure 7: Calibration using selected events greater than magnitude 5.5. Green events are events used in second iteration of least squares linear curve fit, red are those discarded after first fit attempt. Blue line shows fit after second iteration, red line shows initial fit. Dashed lines are 0.5 magnitude units from final curve fit (blue line).

indicates that stacked amplitude can be used as a good proxy for moment magnitude. In Figures 8 through 10 we show the difference in location, origin time and magnitude of the locator results as compared to the NEIC catalog. In these figures we show the results of all events, and not only those that were selected for the calibration. Magnitudes usually fall with 0.2 units of catalog magnitude, the location of 80% of the events is within two grid spacings (i.e. 200 km) from the catalog location and 80% of the origin time measurements are within three time steps (180 seconds). For larger events, this location and time difference is probably at least partly due to the fact that the locator determines a parameter more similar to a centroid, and not epicenter. We also show, in Figure 11, the geographic distribution of events colored according to magnitude difference. There appear to be no systematic patterns, which could have been due, for example, to the uneven station spacing across the globe. Most poorly determined magnitudes are caused by the already discussed problems of interference with the surface waves from previous earthquakes, as well as earthquake depths greater than 150 km. Based on our analysis, we conclude that the prototype system performs well, especially for events greater than magnitude 6. Unfortunately, there is no near real-time catalog available to us for comparison with our results. The catalogs used in the movies generated by the system were obtained at the time the system was initiated, which means that the earliest events had occurred more than 24 hours ago, and therefore in all likelihood had already been updated in the catalog based on more detailed analysis and human review, such as the GCMT analysis or HYDRA analyst review. Therefore at this point in time no systematic comparison of the performance of our system to that of the other near real-time NEIC techniques with similar delay times (on the order of 30 minutes) is possible. Based on incidental data, we believe that our prototype system performs as well or better than most other real-time techniques, especially those that are body wave based, in particular for large earthquakes, as well as transform earthquakes.

Development of determination of moment tensors and depths

The inversion of measurements of complex spectra of long period surface waves, in particular Rayleigh waves, is a well-established method to obtain the source mechanism of local, regional or teleseismic earthquakes. Because the particular application in this case calls for a rapid assessment of the moment tensor in a continuous real-time environment, we have chosen a very efficient spectral inversion algorithm originally developed by Kanamori and Given (1981) and subsequently extended by Thio and Kanamori (1995, 1996). As Kanamori and Given (1981) demonstrated, this spectral method with long-period surface waves works well for events larger than $M=6$ using global recordings (in their case the IDA network). This particular implementation

uses an asymptotic approximation to the normal mode formulation of seismic waves and inverts the complex spectra of surface waves for a moment tensor. Following Kanamori and Given, a complex surface wave spectrum ($V(r,\omega)$), corrected for propagation and attenuation effects, can be written as:

$$V(r,\omega) = \left\{ -P_R \left[M_{xy} \sin 2\varphi - \frac{1}{2}(M_{yy} - M_{xx}) \cos 2\varphi \right] - \frac{1}{2}S_R(M_{yy} + M_{xx}) + iQ_R(M_{yz} \sin \varphi + M_{xz} \cos \varphi) \right\}$$

where φ is the azimuth to the station, P, S and Q are excitation functions. This linear equation is usually solved for the moment tensor elements (M) using traditional least-squares methods.

This particular method is very suitable for our purposes since the input data (i.e. complex spectra) have already been computed by the locator algorithm. The extra load on the system is therefore minimal, especially since the inversion typically only uses spectra at four or five periods per station. Since the locator algorithm already searches over centroid location and time, there is no need to separately invert for that in the moment tensor inversion. The only parameter, in addition to the moment tensor elements, that is not constrained by the locator is the event depth.

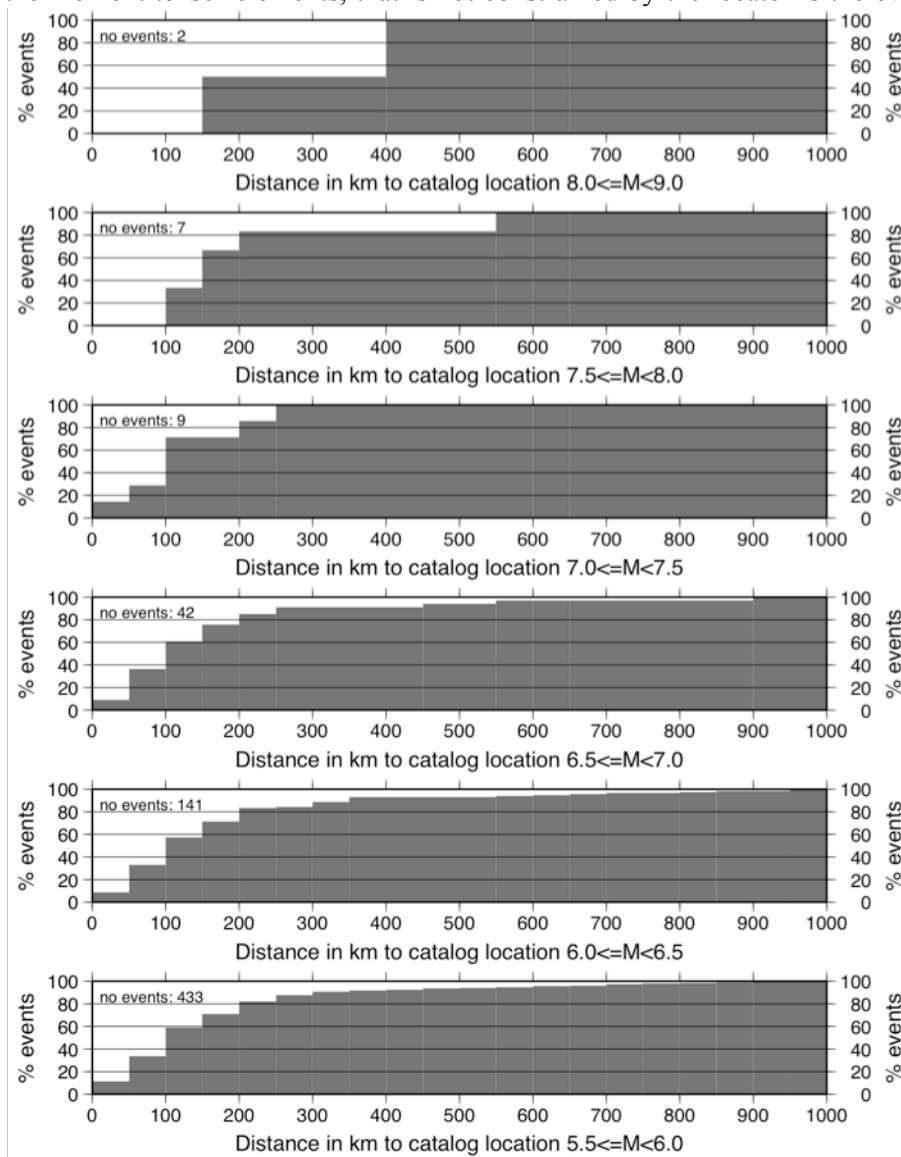


Figure 8: Histograms of distance in km between determined location and final NEIC catalog location for different magnitude ranges.

Thio and Kanamori (1995) determined the centroid depth using this method by a grid search, which simply consists of a linear MT inversion for a predetermined set of depths and choosing the solution with the highest variance reduction. For this system the calculation of MT and depth are carried out continuously on a global grid. Thus, the system produces a global grid of moment tensors and depth, with a high variance reduction value indicating those grid points that correspond to a “real” earthquake.

We show an example of a moment tensor inversion using the spectrograms from the locator algorithm for the 2006 Hawaii event in Figure 12. For this example, we ran 20 separate inversions for 10 different periods at depths between 1 and 40 km. The best solution is at a depth of 25 km as indicated by the minimum in the variance. The main mechanism and the radiation patterns (center panels) are shown for this best fitting depth. A significant magnitude dependence on depth exists, with the moment magnitude at the best fitting depth equal to $M_w=6.7$ (see left hand panel). The mechanism on the other hand appears to be relatively stable with depth (see right hand panel). Mechanism, magnitude and depth are all consistent with the Global CMT

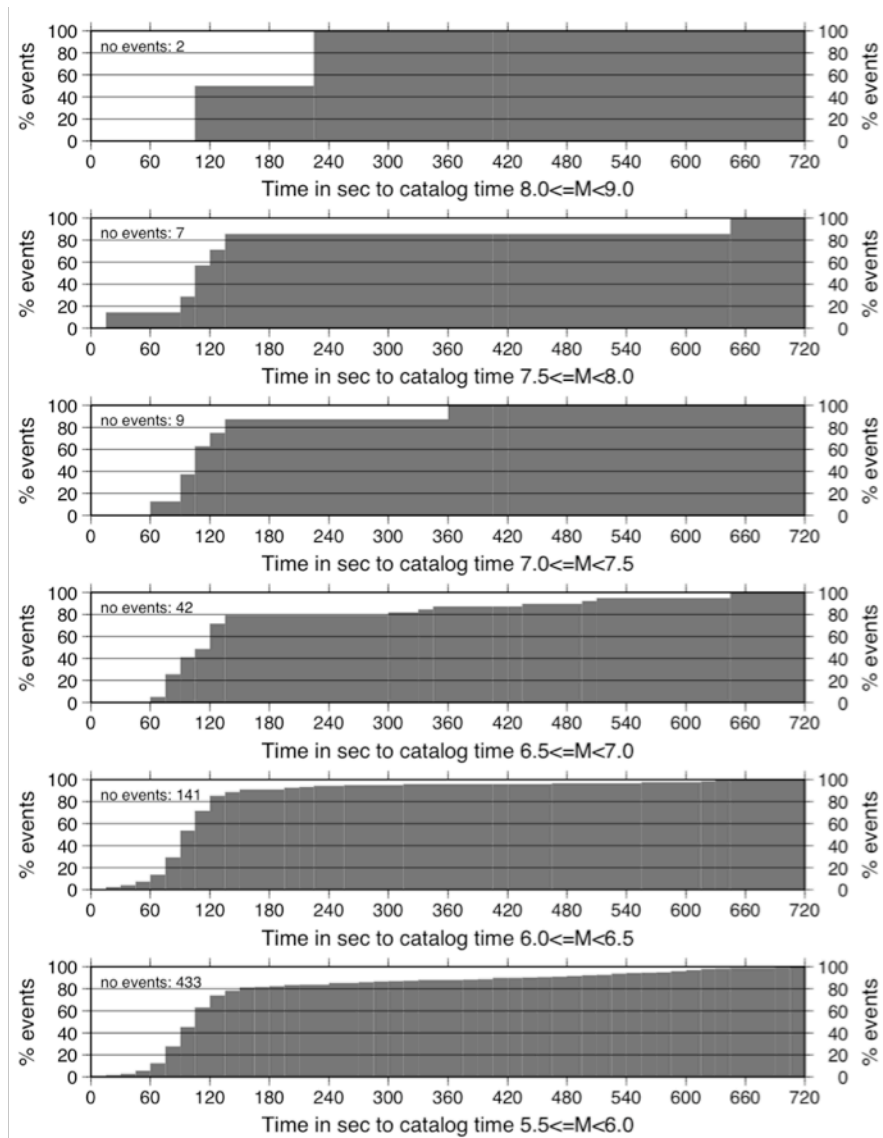


Figure 9: Histograms of time difference in seconds between determined origin time and final NEIC catalog origin time for different magnitude ranges.

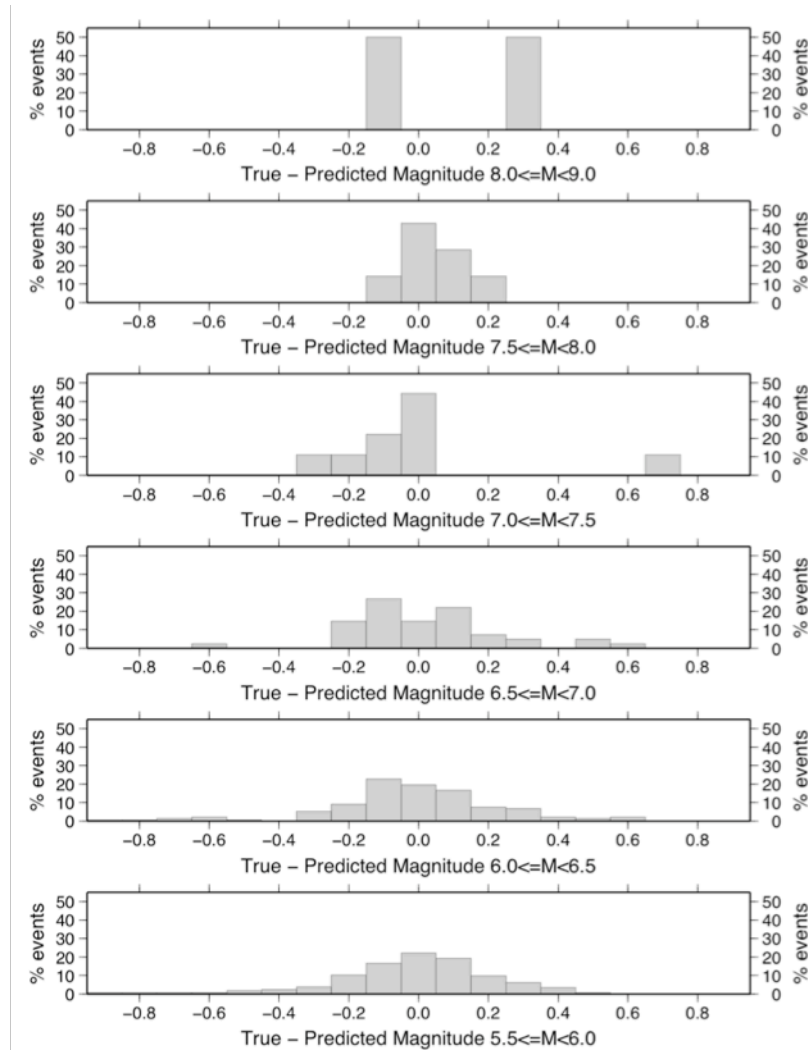


Figure 10: Histograms of magnitude difference between determined magnitude (calculated from maximum stacked amplitude using calibration parameters) and final NEIC catalog magnitude for different magnitude ranges.

solution. The CPU time for the entire suite of 20 inversions is .035 sec.

Since the locator algorithm consists mainly of mappings from one space to another it is highly efficient. The system been installed at the NEIC is running satisfactorily on a Mac mini. Since the algorithm can be operated continuously, and no special measures have to be taken if events are detected, the load on the system can be constant and therefore it is unlikely to run into performance problems during times of increased seismicity. The calculation of a continuous moment tensor on a global scale would also not be prohibitive in terms of computational expenses, as our example for the Hawaii earthquake shows. Since the spacing in time for the global locator is on the order of one minute, we could invert for hundreds of moment tensors without lagging behind the operation of the locator in near real-time. We have however initially restricted the number of grid points for which moment tensors are computed to those grid points that represent a maximum of the stacked amplitude on the globe.

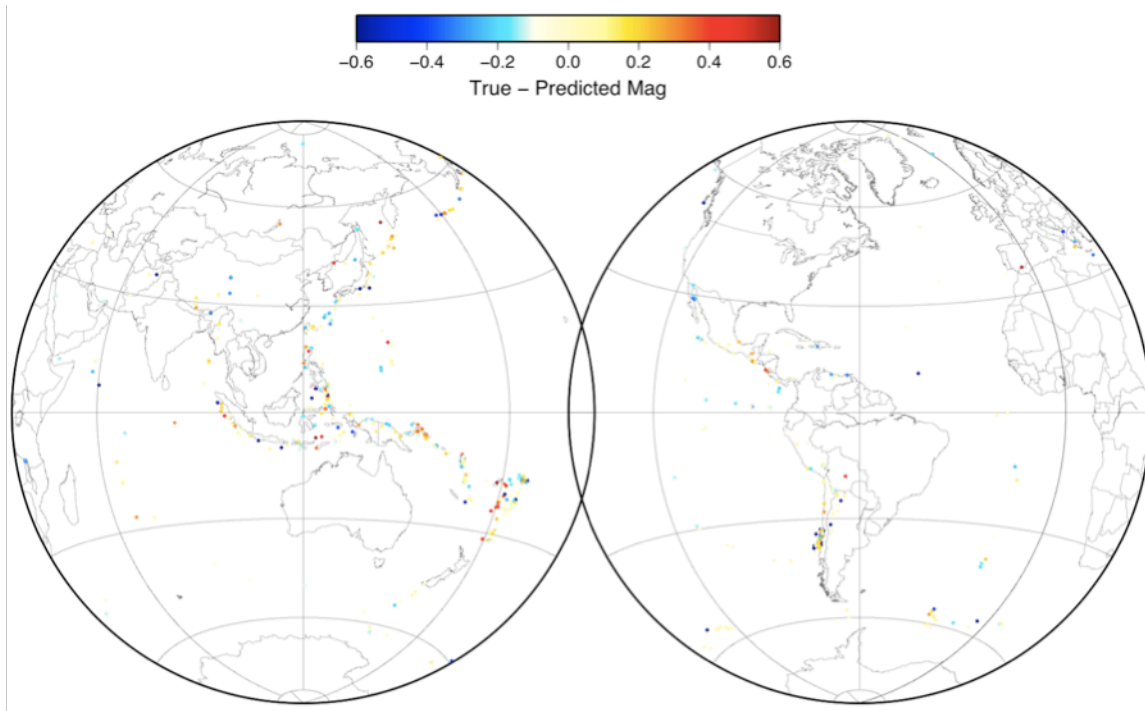


Figure 11: Geographical distribution of events colored according to magnitude difference with final NEIC catalog.

Current status of determination of moment tensors and depths

We have tested our new moment tensor module on a selection of recent large events (Figure 13). The moment tensors calculated by the algorithm generally agree well with the GCMT solutions, as do the calculated magnitudes. We should note that both the original locator algorithm and the new moment tensor module underestimate the magnitude of the largest event in the catalog, the 2010 Chile earthquake. This may be partly due to the fact that this event (as shown by preliminary analyses) appears to consist of two sub-events that have a significant time and spatial separation.

The depth calculated by this method, through the use of a grid search, is only approximately determined due to the long period nature of the input data, but allows for the distinction between crustal (0-40 km) and deeper events (Figure 14). Although the results of our initial analysis are promising, the currently implemented version of our system would in all likelihood not be able to accurately determine moment tensors for events smaller than $M_w 7.5$. This limitation is due to the coarse grid spacing (1 degree) and time step (1 minute) currently used. Since the moment tensor module inverts the variation of phase as well as amplitude with azimuth for the moment tensor elements, it is sensitive to the phase error introduced by this level of imprecision in earthquake location and origin time. This issue is particularly significant for smaller events, because these events require the use of shorter periods, which will be more affected by these phase errors. However, this problem may be addressed by performing additional calculations, in effect creating a denser grid in space and time, for those location/time pairs for which an event has been detected. This approach would go against the constant load methodology that is preferable in a near real-time context, and with the continuing increase in computational power a valid alternative may be to create a more dense global grid and to use smaller time steps to improve the overall analysis of earthquake parameters, including location, origin time and magnitude.

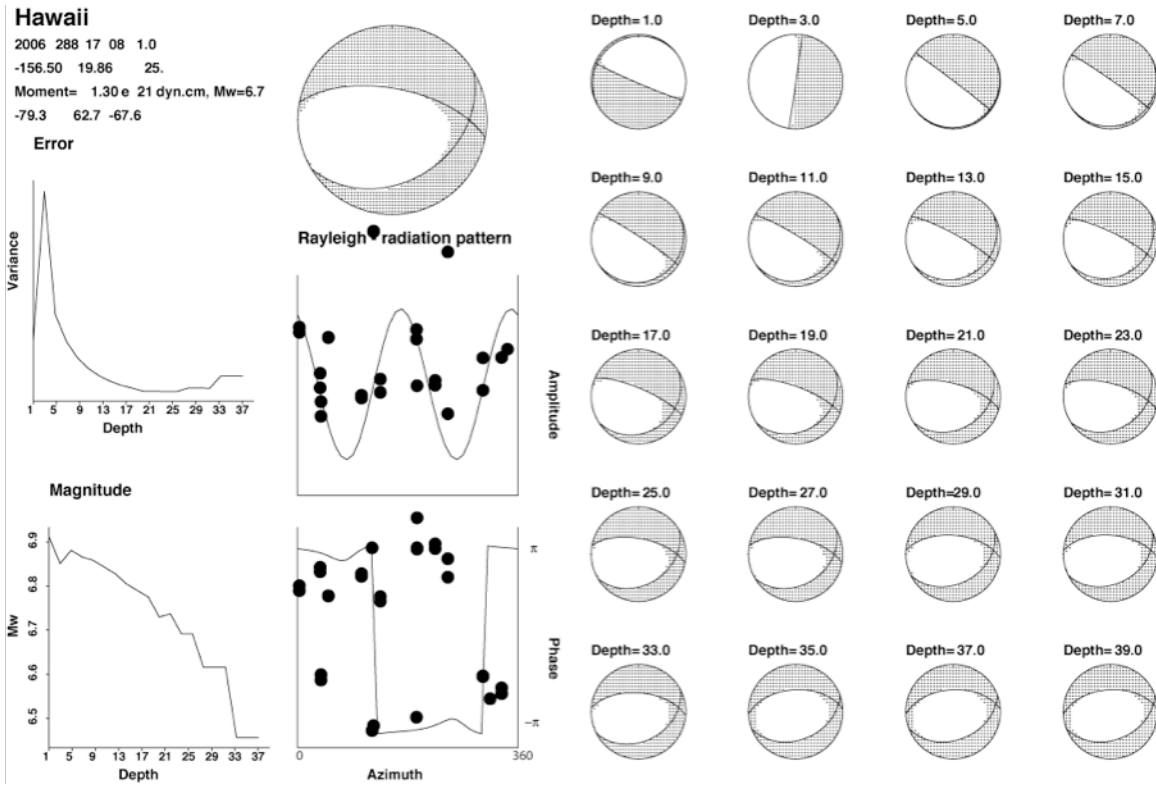


Figure 12. Example of a moment tensor inversion for the 2006 M_w 6.7 Hawaii event, based on 20 separate inversions for 10 different periods and depths between 1 and 40 km. The best solution is at a depth of 25 km as indicated by the minimum in the variance, and the mechanism and radiation pattern are shown for this depth and a period of 150 sec.

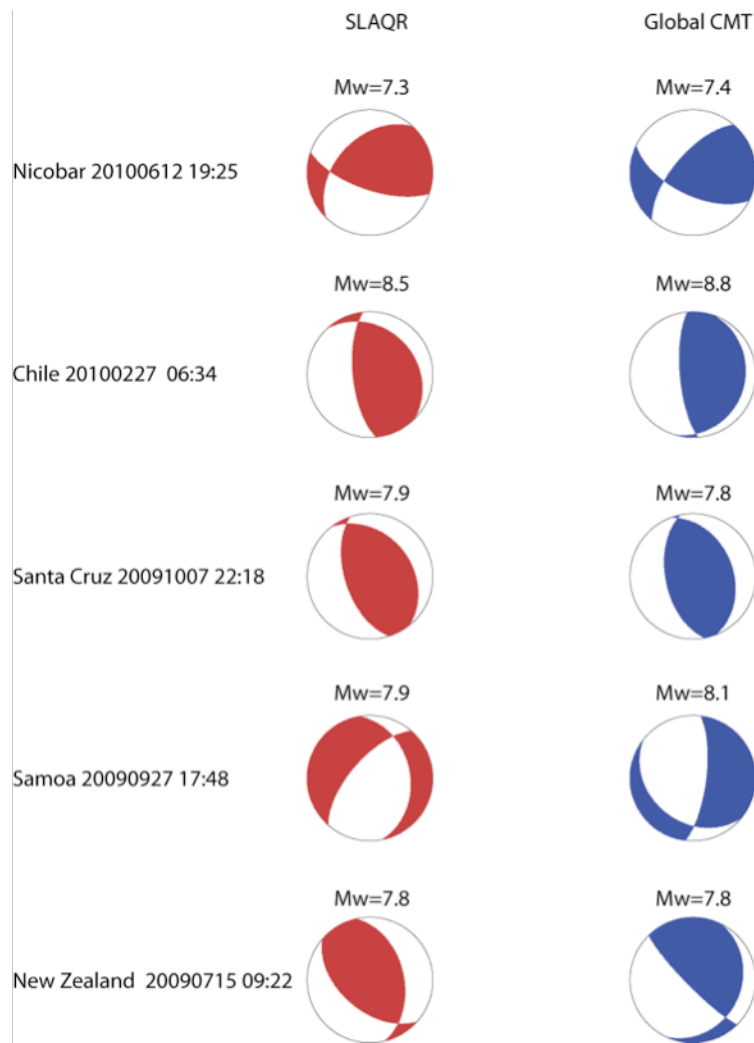


Figure 13. Comparison of moment tensors calculated by the new moment tensor module of the surface wave back-projection system (left and red) with the GCMT mechanisms (blue and right) for a selection of recent large events. Note that only double couple mechanisms could be plotted and that the full moment tensors are even more similar in appearance.

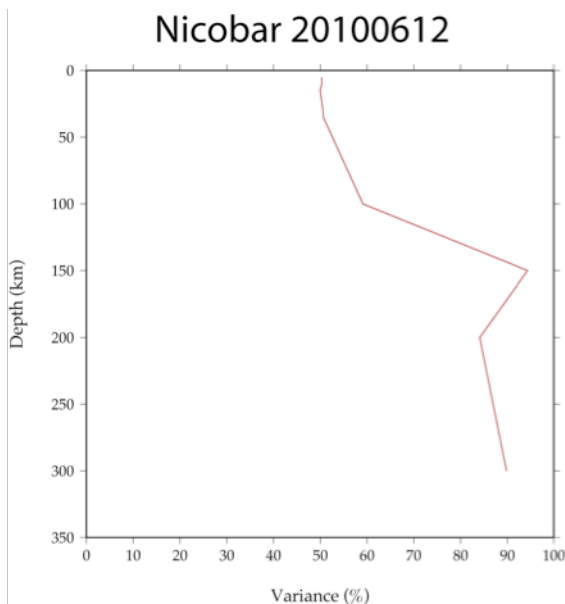


Figure 14. Results of depth search for Nicobar event also shown in Figure 13. Although overall depth resolution is poor, analysis indicates event is crustal in nature.

References

- Ammon, C.J., C. Ji, H.K. Thio, D. Robinson, S. Ni, V. Hjorleifsdottir, H. Kanamori, T. Lay, S. Das, D. Helmberger, G. Ichinose, J. Polet and D. Wald; Rupture Process of the 2004 Sumatra-Andaman Earthquake, *Science*, 308, 1133-1139, 2005.
- Beroza, G.C. and T.H. Jordan, 1990. Searching for slow and silent earthquakes using free oscillations, *J. Geophys. Res.*, 95, 2485-2510.
- Chen, X., Shearer, P.M., Walker, K.T., Fricker, H.A., 2008. Global Seismic Event Detection Using Surface Waves: 15 Possible Antarctic Glacial Sliding Events, Abstract, American Geophysical Union, Fall Meeting.
- Ekström, G. and M. Nettles, 2002, Detection and location of slow seismic sources using surface waves, *EOS* 83, F1037.
- Ekström, G., M. Nettles, and G.A. Abers, 2003. Glacial earthquakes, *Science*, 302, 622-624.
- Ishii, M., Shearer, P.M., Houston, H., & Vidale, J.E., 2005. Extent, duration and speed of the 2004 Sumatra-Andaman earthquake imaged by the Hi-Net array. *Nature* 435(7044), 933-936, doi10.1038/nature03675.
- Ihmlé, P.F. and Thomas H. Jordan Teleseismic Search for Slow Precursors to Large Earthquakes, *Science* **266** (5190), 1547.
- Ito, Y., Obara, K., Shiomi, K., Sekine, S. and H. Hirose, 2007. Slow Earthquakes Coincident with Episodic Tremors and Slow Slip Events, *Science*, 315, 503-506.
- Kanamori, H., and Given, J.W., 1981, Use of long-period surface waves for rapid determination of earthquake source parameters: *Phys. Earth Planet. Int.*, v. 27, p. 8-31. .
- Kawakatsu, H. 1998. On the real-time monitoring of long-period seismic wavefield, *Bull. Earthq. Res. Inst.*, 73, 267-274.
- Kawakatsu, H. 2002. On the realtime monitoring of the long-period seismic wavefield, in *Methods and applications of signal processing in seismic network operations*, edited by T. Takanami and G. Kitagawa, Springer, 266pp, 251-257.
- McGuire, J.J., P. F. Ihmlé, and T. H. Jordan, 1996. Time-Domain Observations of a Slow Precursor to the 1994 Romanche Transform Earthquake, *Science* **274** (5284), 82.
- Polet, J. and H. Kanamori; Shallow subduction zone earthquakes and their tsunamigenic potential, *Geophys. Journ. Int.*, 684-702, 2000.
- Polet, J. and H.K. Thio, 2003. The 1994 Java tsunami earthquake and its 'normal' aftershocks, *Geophysical Research Letters*, 30, 1474, doi:10. 1029/2002GL016806.
- Ronchi, C R. Iacono, M.V. Struglia, A. Rossi, C. Truini, P.S. Paolucci and S. Pratesi, 1996. The Cubed Sphere: a new method for solving PDEs on the sphere. Applications to climate modeling and planetary circulation problems, *Proceedings of parallel computational fluid dynamics 96*, Elsevier Science Publishers, The Netherlands.
- Shearer, P., 1994. Global seismic event detection using a matched filter in long-period seismograms, *J. Geophys. Res.*, 99, 13,713-13,725.
- Tajima, F., C. Megnin, D. Dreger, and B. Romanowicz, 2002. Feasibility of Real-Time Broadband Waveform Inversion for Simultaneous Moment Tensor and Centroid Location Determination, v. 92; no. 2; p. 739-750; DOI: 10.1785/0120000294.
- Thio, H.K., and H. Kanamori, 1995. Moment tensor inversion for local earthquakes using surface waves recorded at TERRAScope, *Bull. Seism. Soc. Am.*, 85, 1201-1238.
- Thio, H.K. and Kanamori, H., 1996. Source complexity of the 1994 Northridge earthquake and its relation to aftershock mechanisms. *Bull. Seismol. Soc. Am.*, 86, S84-S92.
- Walker, K.T., Ishii, M. and P.M. Shearer, 2005. Rupture details of the 28 March 2005 Sumatra Mw 8.6 earthquake imaged with teleseismic P waves, *Geophys. Res. Lett.*, 32, L24303, doi:10.1029/2005GL024395.